Inorganic Chemistry

ARTICLE

pubs.acs.org/IC

Cobalt and Manganese Diphosphonates with One-, Two-, and Three-Dimensional Structures and Field-Induced Magnetic Transitions

Deng-Ke Cao,* Mei-Juan Liu, Jian Huang, Song-Song Bao, and Li-Min Zheng*

State Key Laboratory of Coordination Chemistry, Cordination Chemistry Institute, School of Chemistry and Chemical Engineering, Nanjing University, Nanjing 210093, P. R. China

Supporting Information

ABSTRACT: Reactions of 2-(1-Imidazole)-1-hydroxyl-1,1′-ethylidenediphosphonic acid ($ImhedpH_4$) and cobalt or manganese salts under hydrothermal conditions result in three new metal diphosphonates: β-$Co_3(ImhedpH)_2(H_2O)_4\cdot 2H_2O$ (**1**), $Co_3(ImhedpH)_2(H_2O)_4$ (**2**), and $Mn(ImhedpH_2)\cdot H_2O$ (**3**). In compound **1**, the columns made up of $\{Co1_2O_2\}$ dimers and $\{PO_3C\}$ tetrahedra through corner-sharing are cross-linked through $\{Co2O_6\}$ octahedra, forming an inorganic layer. Neighboring layers are pillared by coordinated imidazole groups of $ImhedpH^-$ ligands, leading to a three-dimensional open framework containing two kinds of channels with sizes of 8.256 × 9.851 Å and 8.030 × 4.745 Å (van der Waals radii not accounted for). Compound **2** shows a layer structure, in which $Co_3(ImhedpH)_2(H_2O)_4$ trimer units are connected through the corner-sharing of $\{Co1O_5\}$ trigonal bipyramids and $\{PO_3C\}$ tetrahedra, forming an inorganic layer containing 20-member rings composed of six Co atoms, two μ_3-O1 units, and four O−P−O units. The noncoordinated imidazole groups protrude from two sides of the layer. Compound **3** shows a ladder structure, where the Mn(II) ions are bridged by $ImhedpH_2^{2-}$ ligands through double O−P−O units to form a single chain, and two such chains are further fused together by sharing edges of $\{MnO_5\}$ trigonal bipyramids. The magnetic properties of **1**−**3** have been studied. Ferrimagnetism and field-induced magnetic transition from ferrimagnetism to a fully polarized state are observed in **1**. Compounds **2** and **3** reveal dominant antiferromagnetic interactions between metal centers, and two-step field-induced magnetic phase transitions are found in **2**.

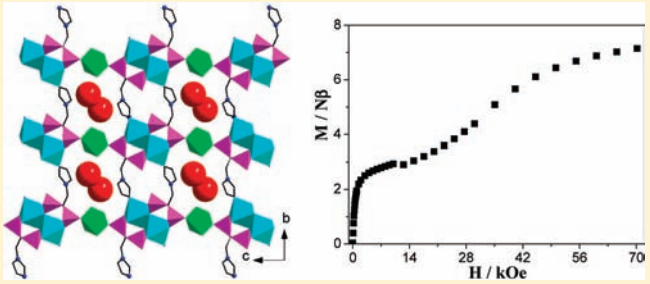

INTRODUCTION

In recent years, considerable effort has been focused on metal phosphonates not only due to their novel architectures but also for their potential applications in exchange and sorption,[1] catalysis,[2] optics,[3] biotechnology,[4] and magnetism. In the study of molecule-based magnetic materials, metal phosphonates could provide good examples for understanding some interesting magnetic phenomena, for example, single molecule magnets,[5,6] single chain magnets,[7] weak ferromagnetism,[8,9] ferrimagnetism,[10] field-induced transition,[11] etc. However, the number of metal phosphonates exhibiting these magnetic phenomena is limited. Therefore, it is still a great challenge to synthesize new metal phosphonates with interesting magnetic properties. Several approaches have been employed to prepare metal phosphonates, such as the choice of suitable phosphonate acid, the introduction of a second ligand,[12] the use of an organic or inorganic template,[13] and the variation of reaction conditions, etc., which resulted in a variety of structures with related physical properties.

2-(1-Imidazole)-1-hydroxyl-1,1′-ethylidenediphosphonic acid ($ImhedpH_4$), also named zoledronic acid, is popularly used to treat a variety of bone resorption diseases.[14] So far, only a limited number of metal phosphonates based on $ImhedpH_4$ have been reported. Because of our interest in molecular magnetism, we previously studied the structures and magnetic properties of Cu, Co, and Ni phosphonates based on $ImhedpH_4$.[9b,10a] Several layer compounds with interesting magnetic behaviors have been obtained, including $Cu_3(ImhedpH)_2\cdot 2H_2O$, showing ferrimagnetism below 5.8 K, and isostructural α-$M_3(ImhedpH)_2(H_2O)_4\cdot 2H_2O$ (M = Co, Ni), with canted antiferromagnetism and relaxation behaviors. Freire et al. reported alkaline earth phosphonates (Mg, Ca, Na, and K) from $ImhedpH_4$ and two mononuclear zinc compounds, $Zn(ImhedpH_3)_2(H_2O)\cdot 2H_2O$ and $Zn(ImhedpH_3)_2(H_2O)_2$.[15] In this paper, we report three new metal phosphonates with different structures, obtained by carefully varying reaction conditions including the temperature, pH value, and metal source, namely, β-$Co_3(ImhedpH)_2(H_2O)_4\cdot 2H_2O$ (**1**), $Co_3(ImhedpH)_2(H_2O)_4$ (**2**), and $Mn(ImhedpH_2)\cdot H_2O$ (**3**) (Scheme 1). Compounds **1**−**3** exhibit

Received: September 25, 2010
Published: February 15, 2011

   dx.doi.org/10.1021/ic1019668 | *Inorg. Chem.* 2011, 50, 2278–2287

Scheme 1

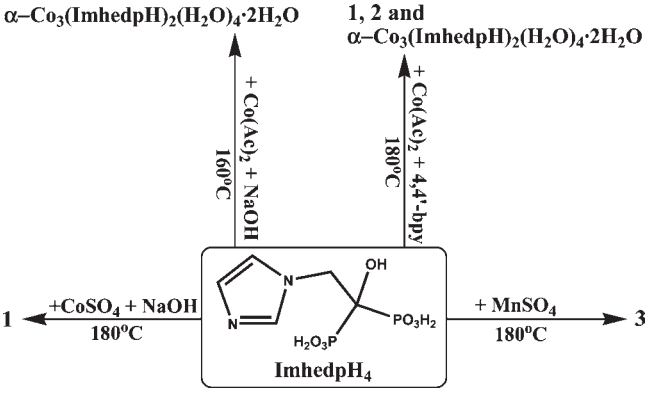

three-, two-, and one-dimensional structures, respectively. The imidazole groups are involved in the coordination with cobalt in **1**, while remaining "free" in compounds **2** and **3**. Their magnetic properties are studied.

EXPERIMENTAL SECTION

Materials and Methods. 2-(1-Imidazole)-1-hydroxyl-1,1′-ethylidenediphosphonic acid ($ImhedpH_4$) was prepared according to the literature method.[16] All other reagents were purchased and used without further purification. Elemental analyses were performed on a Perkin-Elmer 240C elemental analyzer. The IR spectra were obtained as KBr disks on a VECTOR 22 spectrometer. Thermal analyses were performed under a N_2 gas flow using a Mettler-Toloedo TGA/DSC instrument (for **1**) or Perkin-Elmer Pyris 1 analyzer (for **2** and **3**). The heating rate was 10 °C/min from room temperature to 800 °C. Magnetic susceptibility data were obtained on microcrystalline samples (3.95 mg for **1**, 6.11 mg for **2**, and 8.35 mg for **3**), using a Quantum Design MPMS-XL7 SQUID magnetometer. Diamagnetic corrections were made for both the sample holder and the compound estimated from Pascal's constants.[17]

Synthesis of β-$Co_3(ImhedpH)_2(H_2O)_4\cdot 2H_2O$ (1). A mixture of $ImhedpH_4$ (0.10 mmol, 0.0272 g) and $CoSO_4\cdot 7H_2O$ (0.15 mmol, 0.0421 g) in 6 mL of H_2O, adjusted to a pH of 4.00 with 1 M NaOH, was kept in a Teflon-lined autoclave at 180 °C for 5 days. After the mixture was cooled to room temperature, pink needlelike crystals were obtained as a monophasic material based on the powder XRD patterns. Yield: 31 mg (75.6%). Anal. found (calcd) for $C_{10}H_{26}Co_3N_4O_{20}P_4$: C, 14.75 (14.59); H, 3.27 (3.18); N, 7.08 (6.81)%. IR (KBr, cm^{-1}): 3555−3290(m, br), 3196−3039(w, br), 2762(w), 1655(w), 1506(w), 1446(m), 1405(w), 1288(w), 1246(w), 1222(w), 1186(s), 1088(s), 1050(m), 1030(m), 1004(m), 943(w), 890(m), 865(m), 844(w), 795(w), 763(w), 684(w), 662(w), 550(m), 508(w), 470(w), 427(w). Thermal analysis revealed a weight loss of 8.8% over the temperature range 25−165 °C, which corresponds to two lattice and two coordination water molecules (calcd. 8.7%). The remaining two coordination waters were removed between 220 and 342 °C (obsd. 4.3%, calcd. 4.4%), followed immediately by the decomposition of the organic ligand and the collapse of the structure.

Synthesis of $Co_3(ImhedpH)_2(H_2O)_4$ (2). A mixture of $ImhedpH_4$ (0.10 mmol, 0.0272 g), $Co(CH_3CO_2)_2\cdot 4H_2O$ (0.10 mmol, 0.0249 g), 4,4′-bipy·$2H_2O$ (0.1 mmol, 0.0192 g), and 6 mL of H_2O was kept in a Teflon-lined autoclave for 5 h at room temperature and then was treated at 180 °C for 5 days. After slow cooling to room temperature, blue blocky crystals were obtained, together with a few of purple blocky and pink needlelike crystals. The latter two compounds were confirmed as the reported layered compounds α-$Co_3(ImhedpH)_2(H_2O)_4\cdot 2H_2O$[9b] and **1**, respectively. The blue blocky crystals were manually selected and were used for physical measurements. Yield: 13 mg (50% based on Co). Anal. found (calcd) for $C_{10}H_{22}Co_3N_4O_{18}P_4$: C, 15.20 (15.26); H, 2.87 (2.82); N, 7.11 (7.12)%. IR (KBr, cm^{-1}): 3406 (m), 3295(m), 3165−2960(w), 1923(w), 1671(w), 1629(w), 1577(m), 1546(m), 1478(w), 1446(w), 1412(w), 1383(w), 1352(w), 1304(m), 1228(w), 1199(m), 1139(s), 1103(s), 1058(s), 1003(s), 977(s), 952(m), 883(m), 841(m), 778(m), 724(m), 687(w), 634(m), 627(m), 565(m), 488(m), 456(w). Thermal analysis shows that the removal of four coordination water molecules (calcd. 9.2%) occurred between 240 and 312 °C, with a weight loss of 9.1%. Above 312 °C, the structure collapsed, and the organic ligand decomposed.

Synthesis of $Mn(ImhedpH_2)\cdot H_2O$ (3). A mixture of $ImhedpH_4$ (0.10 mmol, 0.0272 g) and $MnSO_4\cdot H_2O$ (0.10 mmol, 0.0169 g) in 6 mL of H_2O, adjusted to a pH of 3.07 with 1 M NaOH, was kept in a Teflon-lined autoclave at 180 °C for 5 days. After slow cooling to room temperature, colorless needlelike crystals were collected as a monophasic material based on the powder XRD pattern. Yield: 22 mg (64.1%). Anal. found (calcd) for $C_5H_{10}N_2O_8P_2Mn$: C, 17.56 (17.51); H, 3.00 (2.94); N, 8.18 (8.17)%. IR (KBr, cm^{-1}): 3291(m), 3169(w), 3140(s), 3112(m), 3015(w), 2832(w), 2201(w), 1678(m), 1580(m), 1546(m), 1483(w), 1444(m), 1405(w), 1385(w), 1294(s), 1237(w), 1162(s), 1127(s), 1101(s), 1090(s), 1058(s), 1034(s), 967(s), 924(s), 874(w), 860(m), 808(w), 778(w), 721(m), 690(m), 631(m), 593(s), 536(w), 515(w), 488(w), 460(m), 424(m). Thermal analysis showed that the release of one lattice water molecule (calcd. 5.20%) occurred between 175 and 280 °C with a weight loss of 5.6%. The further weight loss above 315 °C is due to the collapse of the structure and the decomposition of the organic ligand.

X-Ray Crystal Structure Studies. Single crystals of dimensions 0.1 × 0.06 × 0.05 mm^3 for **1**, 0.1 × 0.08 × 0.06 mm^3 for **2**, and 0.2 × 0.1 × 0.1 mm^3 for **3** were used for structural determinations on a Bruker SMART APEX CCD diffractometer using graphite-monochromatized Mo Kα radiation (λ = 0.71073 Å) at room temperature. A hemisphere of data was collected in the θ range of 2.18−25.00° for **1**, 2.09−25.49° for **2**, and 2.08−25.50° for **3** using a narrow-frame method with scan widths of 0.30° in ω and an exposure time of 10 s/frame. Numbers of observed and unique [$I > 2\sigma(I)$] reflections are 3032 and 2054 (R_{int} = 0.0436) for **1**, 6790 and 2084 (R_{int} = 0.0459) for **2**, and 5245 and 1995 (R_{int} = 0.0393) for **3**, respectively. The data were integrated using the Siemens *SAINT* program,[18] with the intensities corrected for Lorentz factor, polarization, air absorption, and absorption due to variation in the path length through the detector faceplate. Multiscan absorption corrections were applied. The structures were solved by direct methods and refined on F^2 by full matrix least-squares using SHELXTL.[19] All of the non-hydrogen atoms were located from the Fourier maps and were refined anisotropically. All H atoms were refined isotropically, with the isotropic vibration parameters related to the non-H atom to which they are bonded. The crystallographic data for compounds **1**−**3** are listed in Table 1, and selected bond lengths and angles are given in Tables 2−4. CCDC 787416−787418 contain the supplementary crystallographic data for this paper. These data can be obtained free of charge from the Cambridge Crystallographic Data Centre via www.ccdc.cam.ac.uk/data_request/cif.

RESULTS AND DISCUSSION

Syntheses. Compounds **1**−**3** were prepared through hydrothermal reactions of $ImhedpH_4$ and corresponding metal sulfates or acetates at 180 °C for 5 days. In the preparations of **1** and **3**, metal sulfates were used and the MSO_4/ligand molar ratio was 1.5:1 for **1**, while it was 1:1 for **3**. The pH values of the reaction mixtures were found to greatly affect the formation of **1** and **3**.

dx.doi.org/10.1021/ic1019668 |*Inorg. Chem.* 2011, 50, 2278–2287

Table 1. Crystallographic Data and Refinement Parameters for 1−3.

	1	2	3
empirical formula	$C_{10}H_{26}Co_3N_4O_{20}P_4$	$C_{10}H_{22}Co_3N_4O_{18}P_4$	$C_5H_{10}MnN_2O_8P_2$
fw	823.02	786.99	343.03
cryst syst	triclinic	monoclinic	monoclinic
space group	$P\bar{1}$	$C2/c$	$P2_1/c$
a (Å)	5.0696(5)	12.496(3)	5.4816(9)
b (Å)	9.6081(10)	9.469(2)	15.899(3)
c (Å)	12.5328(13)	19.485(4)	12.6013(19)
α (deg)	89.120(2)		
β (deg)	85.5080(10)	90.14	99.999(3)
γ (deg)	76.862(2)		
V (Å^3)	592.66(10)	2305.5(8)	1081.5(3)
Z	1	4	4
ρ_{calcd} (g cm^{-3})	2.306	2.509	2.107
F (000)	415	1580	692
goodness-of−fit on F^2	0.997	1.060	1.040
R_1, wR_2 $[I > 2\sigma(I)]^a$	0.0383, 0.0651	0.0363, 0.0894	0.0431, 0.0986
R_1, wR_2 (all data)^a	0.0610, 0.0702	0.0515, 0.1017	0.0597, 0.1038
$(\Delta\rho)_{max}$, $(\Delta\rho)_{min}$(e Å^{-3})	0.681, −0.548	0.569, −0.520	0.700, −0.469

$^a R_1 = \Sigma||F_o| - |F_c||/\Sigma|F_o|$. $wR_2 = [\Sigma w(F_o^2 - F_c^2)^2/\Sigma w(F_o^2)^2]^{1/2}$.

For compound **1**, the reaction mixture with a pH value in the range of 3.48−4.45 yields the pure phase of the sample, but a pH value in the range of 3.03−3.48 results in a mixture of **1** and a small amount of purple blocky crystals of α-$Co_3(ImhedpH)_2(H_2O)_4\cdot 2H_2O$,[9b] and a pH above 4.45 leads to a flocculent mixture. For compound **3**, a pure phase can be obtained in the pH range of 2.75−3.45, and additional flocculent impurities were formed above the pH of 3.45. The samples with the best crystal quality and relative high yield can be obtained using a pH of 4.00 for **1** and 3.07 for **3**, respectively. Compound **2** was obtained through the reaction of $ImhedpH_4$, $Co(CH_3CO_2)_2$, and 4,4′-bipy. It was found that the absence of 4,4′-bipy would result in a mixture of α-$Co_3(ImhedpH)_2(H_2O)_4\cdot 2H_2O$ and **1** without the formation of **2**. We failed in preparing the pure phase of **2** because its crystallization is always accompanied by the formation of α-$Co_3(ImhedpH)_2(H_2O)_4\cdot 2H_2O$[9b] and **1** when the molar ratio of $Co(CH_3CO_2)_2$/ligand/4,4′-bipy is (1−1.5):1:(0.5−1.5). Compound **2**, with the best crystal quality and relative high yield, was prepared when the $Co(CH_3CO_2)_2$/ligand/4,4′-bipy molar ratio was 1:1:1.

Crystal Structure of 1. Compound **1** crystallizes in triclinic space group $P\bar{1}$. Its building unit contains one Co1 atom, half a Co2 atom, one $ImhedpH^-$ ligand, and two coordination and one lattice water molecule (Figure 1). Both Co1 and Co2 atoms display a distorted octahedral geometry. Around the Co1 atom, two of six coordination sites are occupied by phosphonate oxygens (O1 and O4) from the same $ImhedpH^-$ ligand, the other four positions are filled with three phosphonate oxygens (O1D, O2A, and O5B) and one imidazole nitrogen, N2C, from four equivalent $ImhedpH^-$ ligands. For the Co2 atom, four of six coordination sites are filled with water molecules (O1W, O2W, O1WE, O2WE), and the remaining two positions are occupied by phosphonate oxygens (O6 and O6E) from two equivalent $ImhedpH^-$ ligands. The Co−O bond lengths are in the range of 2.037(3)−2.179(3) Å, in agreement with those in layered compound α-$Co_3(ImhedpH)_2(H_2O)_4\cdot 2H_2O$ [2.001(3)−2.180(3) Å].[9b]

In compound **1**, each $ImhedpH^-$ molecule serves as a heptadentate ligand, using five of six phosphonate oxygen atoms (O1, O2, O4, O5, O6) and one imidazole nitrogen atom N2 to coordinate with six Co atoms (Scheme 2a). The remaining phosphonate oxygen atom O3 is protonated [P1−O3 = 1.584(3) Å]. The phosphonate oxygen O1 serves as a μ_3-O and links two equivalent Co1 atoms (Co1 and Co1D) into a $\{Co1_2O_2\}$ dimer with a Co···Co distance of 3.289 Å and a Co1−O1−Co1D bond angle of 98.14(14)°. These dimers are further connected by four $\{PO_3C\}$ tetrahedra from two equivalent $ImhedpH^-$ ligands, forming a column along the a direction (Figure 2, top). The phosphonate oxygens O6 and O6E from neighboring columns coordinate to one Co2 atom, hence forming a layered structure, in which columns are cross-linked through $\{Co2O_6\}$ octahedra (Figure 2, bottom). These layers are pillared by imidazole groups of $ImhedpH^-$ ligands with an interlayer distance of 9.357 Å due to the coordination of imidazole nitrogen atom N2 to the Co1 atom from the other layer, therefore leading to a three-dimensional open framework containing two kinds of channels with sizes of 8.256 × 9.851 Å and 8.030 × 4.745 Å (van der Waals radii not accounted for) (Figure 3). It is interesting that the former kind of channel is filled with lattice water molecules, but the latter is empty. Extensive hydrogen bonds are observed among coordination/lattice water molecules, phosphonate oxygens, hydroxyl oxygen, and imidazole nitrogen with O···O(N) distances of 2.731 Å (O1W···O4), 2.959 Å (O2W···O6), 2.966 Å (O1W···O3W^a), 2.967 Å (O2W···O1W^b), 2.982 Å (O3···N2^c), and 2.638 Å (O7···O5^d) (symmetry codes: (a) $-x+1, -y, -z+1$, (b) $x+1, y, z$, (c) $-x, -y+1, -z+1$, (d) $x-1, y, z$).

Crystal Structure of 2. Compound **2** crystallizes in monoclinic space group $C2/c$. It has a trimer building unit containing two independent Co atoms (Co1 and Co2) (Figure 4). The Co1 atom has a distorted trigonal bipyramidal geometry. Three basal sites are provided by one water molecule (O1W) and two phosphonate oxygens (O2, O3A) from two equivalent

dx.doi.org/10.1021/ic1019668 |Inorg. Chem. 2011, 50, 2278–2287

Table 2. Selected Bond Lengths [Å] and Angles (deg) for 1[a]

Co1−O1	2.175(3)	Co2−O2W	2.155(4)
Co1−O4	2.097(3)	P1−O1	1.509(4)
Co1−O2A	2.051(3)	P1−O2	1.490(4)
Co1−O5B	2.083(3)	P1−O3	1.584(3)
Co1−N2C	2.151(4)	P2−O4	1.513(3)
Co1−O1D	2.179(3)	P2−O5	1.511(3)
Co2−O6	2.037(3)	P2−O6	1.522(3)
Co2−O1W	2.136(4)		
O2A−Co1−O4	96.33(13)	P2−O5−Co1F	148.4(2)
O2A−Co1−O1	92.58(13)	O6−Co2−O6E	180.00(9)
O4−Co1−O1	91.10(13)	O6−Co2−O1W	90.92(13)
O2A−Co1−O5B	176.99(14)	O6E−Co2−O1W	89.08(13)
O5B−Co1−O1	85.30(13)	O6−Co2−O1WE	89.08(13)
O5B−Co1−O4	85.86(12)	O6E−Co2−O1WE	90.92(13)
O2A−Co1−N2C	86.12(15)	O1W−Co2−O1WE	180.0(3)
O5B−Co1−N2C	96.03(15)	O6−Co2−O2W	89.74(14)
O4−Co1−N2C	88.20(14)	O6E−Co2−O2W	90.26(14)
N2C−Co1−O1	178.45(15)	O1W−Co2−O2W	94.13(16)
O2A−Co1−O1D	90.74(13)	O1WE−Co2−O2W	85.87(16)
O5B−Co1−O1D	86.84(12)	O6−Co2−O2WE	90.26(14)
O4−Co1−O1D	170.26(13)	O6E−Co2−O2WE	89.74(14)
N2C−Co1−O1D	98.99(14)	O1W−Co2−O2WE	85.87(16)
O1−Co1−O1D	81.86(14)	O1WE−Co2−O2WE	94.13(16)
P1−O1−Co1	132.33(19)	O2W−Co2−O2WE	180.0(2)
P1−O1−Co1D	128.30(19)	P2−O6−Co2	136.7(2)
Co1−O1−Co1D	98.14(14)	C1−N2−Co1G	125.7(4)
P1−O2−Co1A	140.8(2)	C2−N2−Co1	128.6(3)
P2−O4−Co1	137.0(2)		

[a] Symmetry transformations used to generate equivalent atoms: (A) $-x+1, -y, -z+1$; (B) $x-1, y, z$; (C) $x, y-1, z$; (D) $-x, -y, -z+1$; (E) $-x+1, -y, -z$; (F) $x+1, y, z$; (G) $x, y+1, z$.

Table 3. Selected Bond Lengths [Å] and Angles (deg) for 2[a]

Co1−O1	2.329(3)	Co2−O3W	2.078(5)
Co1−O2	2.063(3)	P1−O1	1.521(3)
Co1−O1W	1.967(4)	P1−O2	1.529(3)
Co1−O3A	2.050(3)	P1−O3	1.524(3)
Co1−O5A	1.954(3)	P2−O4	1.523(3)
Co2−O1	2.076(3)	P2−O5	1.525(3)
Co2−O4	2.075(3)	P2−O6	1.518(3)
Co2−O2W	2.127(4)		
O2−Co1−O1	66.36(11)	O3W−Co2−O1	94.12(8)
O1W−Co1−O2	141.67(13)	O1B−Co2−O1	171.76(17)
O5A−Co1−O1W	99.75(13)	O3W−Co2−O4	90.54(9)
O5A−Co1−O3A	97.17(12)	O1B−Co2−O4	89.93(11)
O1W−Co1−O3A	108.62(13)	O1−Co2−O4	90.00(11)
O5A−Co1−O2	104.55(13)	O4−Co2−O4B	178.92(17)
O3A−Co1−O2	97.33(12)	O3W−Co2−O2W	180.000(1)
O5A−Co1−O1	168.18(11)	O1−Co2−O2W	85.88(8)
O1W−Co1−O1	84.75(12)	O4−Co2−O2W	89.46(9)
O3A−Co1−O1	91.65(10)	P1−O1−Co2	135.70(17)
P1−O1−Co1	88.64(14)	Co2−O1−Co1	126.43(14)
P1−O2−Co1	98.92(16)	P2−O4−Co2	135.84(17)

[a] Symmetry transformations used to generate equivalent atoms: (A) $-x+1/2, y-1/2, -z+1/2$; (B) $-x, y, -z+1/2$; (C) $-x+1/2, y+1/2, -z+1/2$.

Table 4. Selected Bond Lengths [Å] and Angles (deg) for 3[a]

Mn1−O1	2.075(3)	O5−Mn1C	2.253(2)
Mn1−O4	2.094(3)	P1−O1	1.505(3)
Mn1−O2A	2.105(3)	P1−O2	1.524(3)
Mn1−O5A	2.253(3)	P1−O3	1.517(3)
Mn1−O5B	2.114(3)	P2−O4	1.499(3)
O2−Mn1C	2.105(3)	P2−O5	1.524(3)
O5−Mn1B	2.114(3)	P2−O6	1.547(3)
O1−Mn1−O4	88.21(10)	O4−Mn1−O5B	102.16(11)
O1−Mn1−O2A	91.29(10)	O5B−Mn1−O5A	79.79(10)
O1−Mn1−O5A	177.36(11)	P1−O1−Mn1	140.40(17)
O1−Mn1−O5B	102.80(11)	P2−O4−Mn1	129.04(15)
O2A−Mn1−O5A	87.61(10)	P1−O2−Mn1C	124.26(16)
O2A−Mn1−O5B	102.10(11)	P2−O5−Mn1B	134.27(16)
O4−Mn1−O2A	155.22(12)	P2−O5−Mn1C	122.27(15)
O4−Mn1−O5A	91.79(9)	Mn1B−O5−Mn1C	100.21(10)

[a] Symmetry transformations used to generate equivalent atoms: (A) $x-1, y, z$; (B) $-x+1, -y+1, -z+2$; (C) $x+1, y, z$.

$ImhedpH^-$ ligands. The Co1 atom deviates from the basal plane by 0.3872 Å. Two axial positions are occupied by phosphonate oxygens (O1, O5A) from two $ImhedpH^-$ ligands, respectively [O1−Co1−O5A = 168.18(11)°]. The Co2 atom adopts a distorted octahedral geometry, with the six sites occupied by two pairs of phosphonate oxygen atoms (O1 and O4; O1B and O4B) and two water molecules (O2W and O3W).

In compound **2**, each $ImhedpH^-$ ligand serves as a hexadentate ligand, using five of six phosphonate oxygens (O1, O2, O3, O4, O5) to coordinate with three Co atoms (Scheme 2b). The pendant phosphonate oxygen O6 [P2−O6 = 1.522(3) Å] and protonated imidazole nitrogen N2 are not involved in coordination. Two equivalent $ImhedpH^-$ molecules chelate and bridge two Co1 and one Co2 atom, forming an $Co_3(ImhedpH)_2(H_2O)_4$ trimer building unit, in which the Co2 atom sitting on the C_2 rotary axis defined by coordination water molecules O2W and O3W is connected to Co1 atom through μ_3-O1 and O1−P1−O2 units (Figure 4). Along the *b* axis, neighboring trimers are connected through phosphonate oxygens O3 and O5 from one trimer chelating to the Co1 atom from the other, therefore resulting in an inorganic layer structure containing a 20-member ring made up of six Co atoms and two μ_3-O1 and four O−P−O units (Figure 5). In this layer, three kinds of Co···Co distances are observed, including a Co1···Co2 distance over μ_3-O1 (3.922 Å), a Co2···Co1C distance over O−P−O (4.704 Å), and a Co1···Co1C distance over O−P−O (5.901 Å). Extensive intralayer hydrogen bonds are observed, including O1W···O4[a] (2.705 Å), O2W···O3[b] (2.728 Å), O2W···O3[c] (2.728 Å), O7···O3[c] (2.703 Å), O3W···O2[d] (2.719 Å), and O3W···O2[e] (2.719 Å). Neighboring layers are further connected through interlayer hydrogen bond interactions [N2···O6[f] = 2.682 Å, O1W···O6 = 2.619 Å] (symmetry codes: (a) $-x, y, -z+1/2$, (b) $x-1/2, y-1/2, z$, (c) $-x+1/2, y-1/2, -z+1/2$, (d) $-x+1/2, y+1/2, -z+1/2$, (e) $x-1/2, y+1/2, z$, (f) $-x+1/2, -y+1/2, -z$, (g) $x, -y+1, z+1/2$; Figure 6). The distance between neighboring layers is 9.742 Å.

Crystal Structure of 3. Compound **3** crystallizes in monoclinic space group $P2_1/c$. As shown in Figure 7, the building unit of **3** contains one Mn1 atom, one $ImhedpH_2^{2-}$ ligand, and one

dx.doi.org/10.1021/ic1019668 |*Inorg. Chem.* 2011, 50, 2278–2287

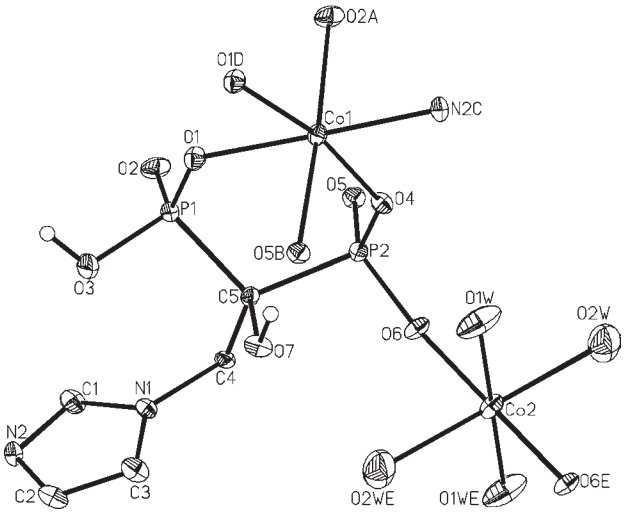

Figure 1. Building unit of **1** with atomic labeling scheme (50% probability). Lattice waters and all H atoms except those attached to O3 and O7 are omitted for clarity.

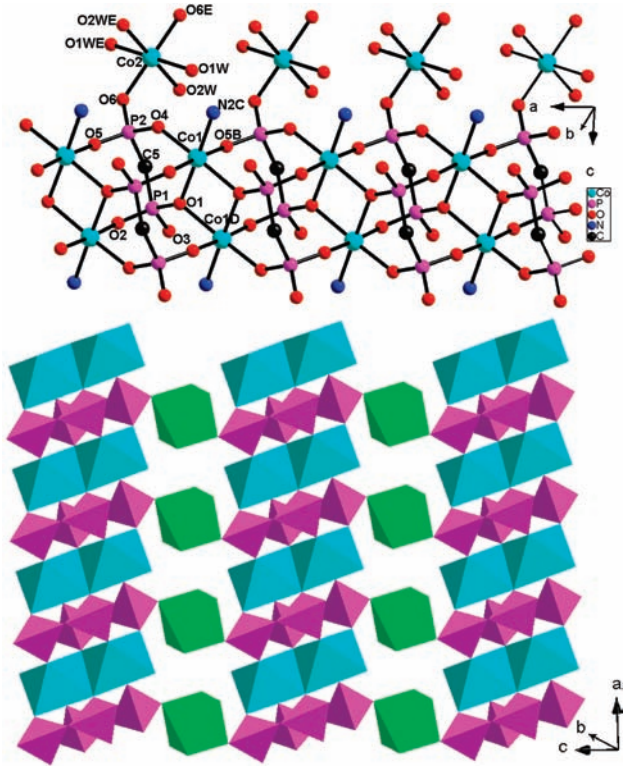

Figure 2. (Top) The column structure in **1**. (Bottom) Polyhedron representation of the inorganic layer in **1**. Color code: $Co1O_6$, cyan; $Co2O_6$, green; PO_3C, purple.

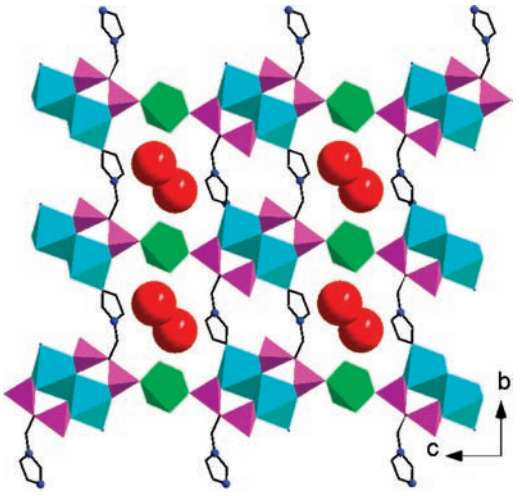

Figure 3. Three-dimensional open framework of **1** containing two kinds of channels. Color code: $Co1O_6$, cyan; $Co2O_6$, green; PO_3C, purple.

Scheme 2

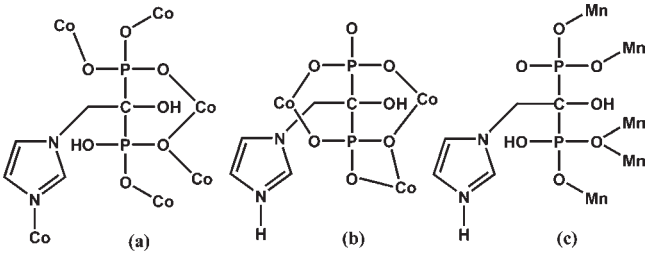

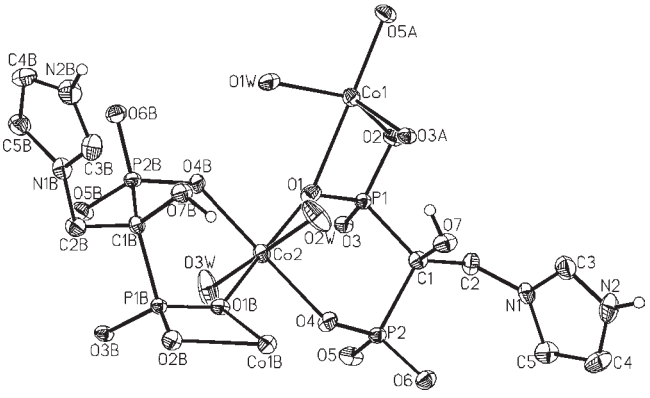

Figure 4. Trimer unit in **2** with atomic labeling scheme (50% probability). All H atoms except those attached to O7, N2, O7B, and N2B are omitted for clarity.

lattice water molecule. The Mn1 atom has a distorted trigonal bipyramidal geometry. Five coordinated sites are occupied by five phosphonate oxygens (O1, O4, O2A, O5A, and O5B) from three equivalent $ImhedpH_2^{2-}$ ligands. The basal plane of the trigonal bipyramid is defined by O4, O2A, and O5B atoms, in which the O−Mn1−O bond angles are in the range of 102.10(11)−155.22(12)°. Two axial positions are occupied by O1 and O5A with an O1−Mn1−O5A bond angle of 177.36(11)°.

Each $ImhedpH_2^{2-}$ behaves as a penta-dentate ligand, using four phosphonate oxygen atoms (O1, O2, O4, and O5) to coordinate with five Mn atoms (Scheme 2c). The remaining two phosphonate oxygen atoms are either pendant [P1−O3 = 1.517(3) Å] or protonated [P2−O6 = 1.547(3) Å]. The Mn(II) ions are bridged by $ImhedpH_2^{2-}$ anions through double O−P−O units (O1−P1−O2, O4−P2−O5), forming an infinite single chain. Two single chains are further cross-linked by the O5 atom

dx.doi.org/10.1021/ic1019668 |*Inorg. Chem.* 2011, 50, 2278–2287

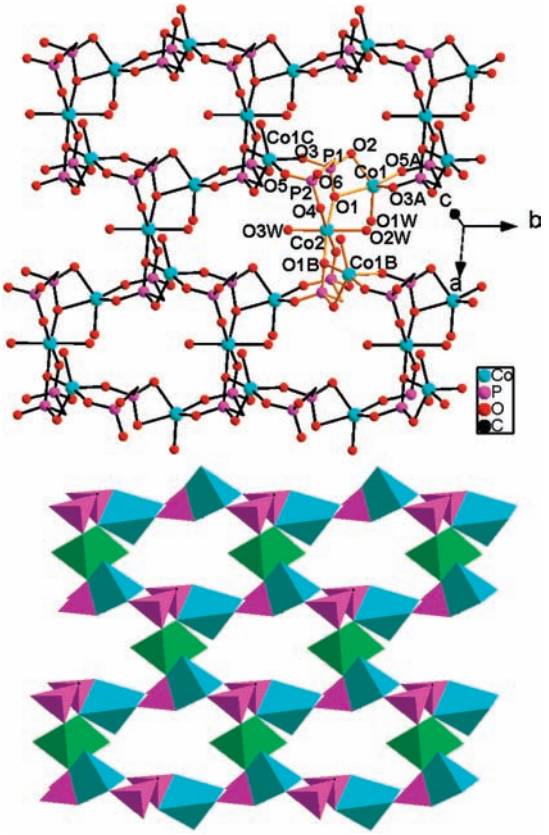

Figure 5. The inorganic layer structure in compound **2**. The connections of neighboring trimer units (top) and the polyhedron representation (bottom). Color code: $Co1O_6$, cyan; $Co2O_6$, green; PO_3C, purple.

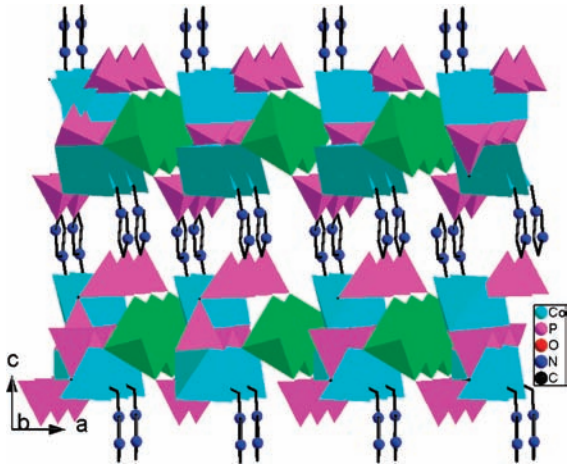

Figure 6. Structure **2** packed along the *b* axis.

serving as μ_3-O, thus leading to a ladder with the edge-sharing $\{Mn_2(\mu_3\text{-}O5)_2\}$ dimers as the rung (Figure 8). The Mn−O5−Mn bond angles are 100.21(10)°. The Mn···Mn distances are 3.351 Å within the dimer and 4.574 and 5.482 Å between the dimers. Neighboring chains are linked together through interchain hydrogen bonds between phosphonate oxygen atoms O3 and O6 [O6···O3^a = 2.501 Å, symmetric code a: $x, -y + 3/2, z + 1/2$], hence forming a three-dimensional network with channels generated along the *a* direction (Figure 9). The

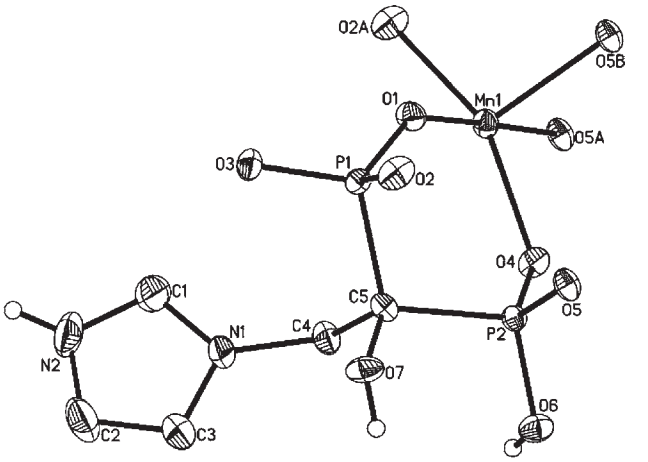

Figure 7. Building unit of compound **3** with atomic labeling scheme (50% probability). Lattice waters and all H atoms except those attached to N2, O7, and O6 are omitted for clarity.

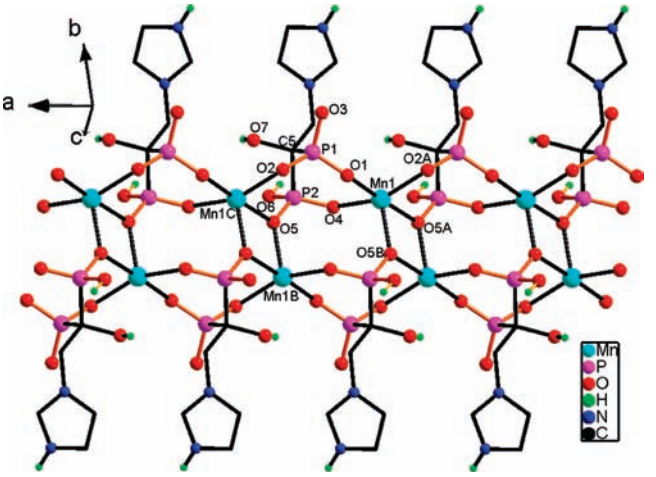

Figure 8. The ladder-like structure of **3**. All H atoms attached to C atoms are omitted for clarity.

protonated imidazole groups and the lattice water fill in these channels and are involved in extensive hydrogen bonds: O1W···O1^b (2.996 Å), O1W···O3^b (2.816 Å), O1W···O2^c (2.921 Å), O7···O1W^d (2.670 Å), N2···O1^e (3.142 Å), and N2···O2^e (3.096 Å) (symmetry codes: (b) $x, -y + 3/2, z - 1/2$; (c) $x - 1, -y + 3/2, z - 1/2$; (d) $x + 1, y, z + 1$; (e) $-x + 1, y + 1/2, -z + 3/2$).

Clearly, compounds **1**−**3** have different structures, in which ligand molecules exhibit three kinds of new coordination modes never observed in reported metal phosphonates based on $ImhedpH_4$.[9b,10a,15] The structures of **1** and **2** are significantly different from that of α-$Co_3(ImhedpH)_2(H_2O)_4\cdot 2H_2O$.[9b] In the latter, neighboring linear $Co_3(ImhedpH)_2(H_2O)_4\cdot 2H_2O$ trimers are connected by edge-sharing of the $\{Co2O_6\}$ octahedra, forming an undulating chain. The adjacent chains are fused through the coordination of the phosphonate oxygen atom from one chain to the Co2 atom of the other, generating a two-dimensional layer containing 4-, 8-, and 16-membered rings. The structural differences among **1**, **2**, and α-$Co_3(ImhedpH)_2(H_2O)_4\cdot 2H_2O$ result from the variation of reaction conditions including temperature, Co source, and the base used for adjusting

dx.doi.org/10.1021/ic1019668 |*Inorg. Chem.* 2011, 50, 2278–2287

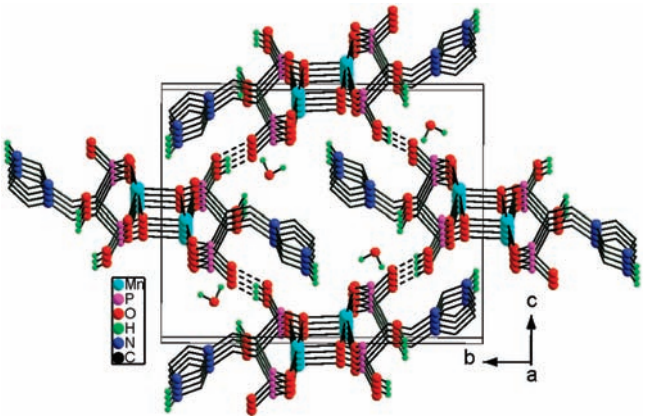

Figure 9. Structure **3** viewed along the *a* axis.

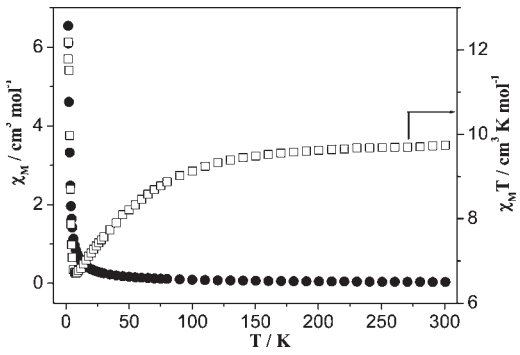

Figure 10. The χ_M and $\chi_M T$ vs T plots for **1**.

the pH value. The chain structure of **3** is similar to some Mn diphosphonates based on $RC(OH)(PO_3H_2)_2$, such as $[NH_3(CH_2)_nNH_3][Mn_2(hedpH)_2]\cdot 2H_2O$ (n = 4−6),[20] $Mn(C_3NH_9P_2O_7)\cdot H_2O$ (R = $-CH_2CH_2NH_2$),[21] and $Mn(ahbdpH_2)$ (R = $-CH_2CH_2CH_2NH_2$).[22] However, the hydroxyl oxygen O7 in **3** is noncoordinated (O7···Mn1C = 2.789 Å in Figure 8); thus, the Mn atom shows a distorted trigonal bipyramidal geometry, while the hydroxyl oxygens in the latter five compounds are involved in coordination, and Mn atoms show octahedral geometry. It indicates that the introduced imidazole group in the diphosphonate ligand could affect the coordination between hydroxyl oxygen (O7) and Mn atom, probably due to space hindrance.

Magnetic Properties. The temperature-dependent magnetic susceptibilities of compound **1** were investigated in the temperature range of 1.8−300 K under 2 kOe. The room-temperature effective magnetic moment per Co_3 unit (8.82 μ_B) is significantly higher than the expected spin-only value for S = 3/2 (6.71 μ_B) due to the orbital contribution of Co(II) ion. The magnetic behavior in the temperature range of 40−300 K follows the Curie−Weiss law with a Weiss constant of −11.00 K and a Curie constant of 10.12 cm^3 K mol^{-1}. Upon cooling from room temperature, $\chi_M T$ decreases gradually to 6.73 $cm^3\cdot K\cdot mol^{-1}$ at 8 K, then increases rapidly to a maximum of 12.18 $cm^3\cdot K\cdot mol^{-1}$ at 2 K, and finally decreases to 11.78 $cm^3\cdot K\cdot mol^{-1}$ at 1.8 K (Figure 10). This corresponds to a typical ferrimagnetic behavior in a system with dominant antiferromagnetic interactions between the Co(II) ions.

In order to determine the existence of a long-range magnetic ordering at low temperatures, temperature-dependent *ac* susceptibility data were measured under H_{ac} = 5 Oe and at a frequency of 10 Hz. Both the in-phase (χ') and out-of phase signals (χ'') increase rapidly upon cooling below 3.0 K (Figure 11). Although no bifurcation is observed in the zero-field-cooled magnetism (ZFCM) and field-cooled magnetism (FCM) curves down to 1.8 K (Figure 11, inset), the *ac* results suggest that the spontaneous magnetization in compound **1** could occur below 3.0 K.

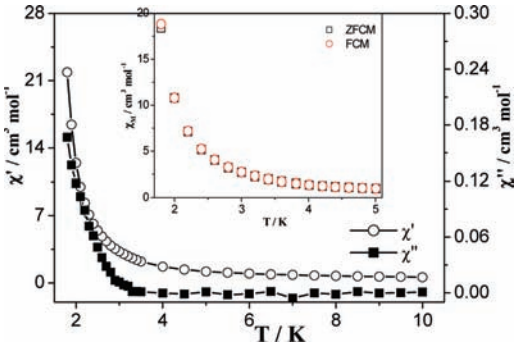

Figure 11. Temperature-dependent zero-field ac magnetic susceptibility for **1**. Inset: ZFCM and FCM curves for **1**.

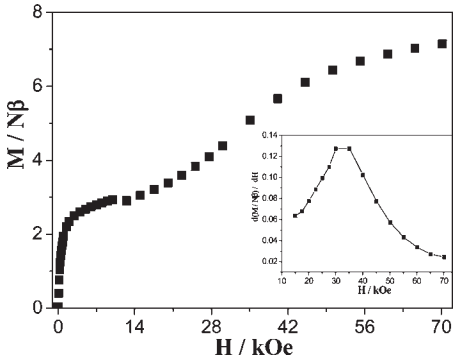

Figure 12. Field-dependent magnetization for **1** at 1.8 K.

It is well-known that the ferrimagnetic behavior in homometallic compounds can result from the odd number of metal atoms in the building unit or complicated alternating sequences of ferro-/antiferro-magnetic interactions.[23] As the structural description of **1**, its building unit contains one Co1 atom and half a Co2 atom. In the inorganic layer, the $\{Co1_2O_2\}$ dimer is linked to the Co2 atom through one O−P−O unit (Figure 2 top). Such connections yield a nonzero net magnetic moment within the antiferromagnetically coupled layer, thus resulting in the ferrimagnetic behavior of compound **1**. A similar situation is also observed in $Cu_3(ImhedpH)_2\cdot 2H_2O$.[10a]

The field-dependent isothermal magnetization measured at 1.8 K reveals that the M per Co_3 displays an abrupt increase to 2.20 Nβ below 1.5 kOe and then slowly reaches 7.14 Nβ at 70 kOe in an *S*-shaped fashion (Figure 12). Considering that the octahedral Co(II) centers have an effective spin S_{eff} = 1/2 and g = 4.1−5.0 at 1.8 K,[23] the magnetization of 2.20 Nβ is near the antiferromagnetic interaction as a consequence of three Co(II) ions ($\Sigma g S_{eff}$ = 2.05−2.5 Nβ), which further confirms the ferrimagnetic behavior in compound **1**. On the other hand, the saturation value of 7.14 Nβ at 70 kOe is in agreement with the anticipated value for three fully spin polarized Co(II) ions (6.15−7.5 Nβ), thus the *S*-shaped magnetization curve above

dx.doi.org/10.1021/ic1019668 |*Inorg. Chem.* 2011, 50, 2278–2287

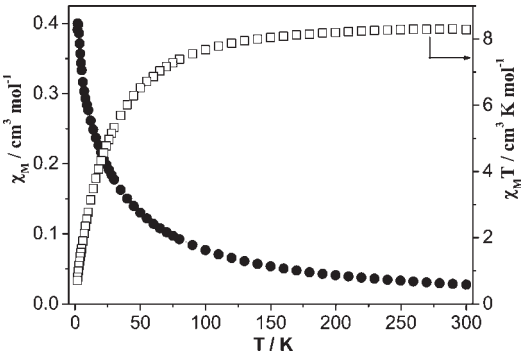

Figure 13. The χ_M and $\chi_M T$ vs T plots for **2**.

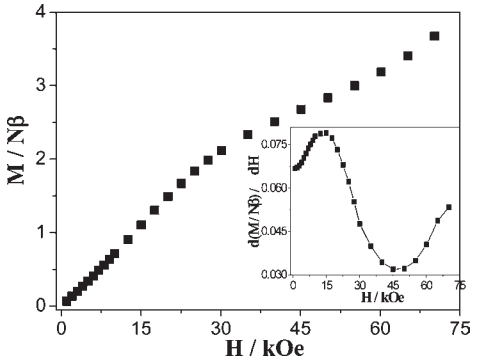

Figure 14. Field-dependent magnetization for **2** at 1.8 K.

1.0 kOe suggests the occurrence of the field-induced magnetic phase transition from ferrimagnetism to a fully polarized state with a critical field of around 32.6 kOe (the inset in Figure 12). In addition, no magnetic hysteresis loop is observed at 1.8 K.

Figure 13 shows the χ_M and $\chi_M T$ versus T plots for compound **2**. The magnetic behavior in the temperature range of 40−300 K follows the Curie−Weiss law with a Weiss constant of −15.77 K and a Curie constant of 8.81 cm^3 K mol^{-1}. The negative Weiss constant and the continuous decrease of $\chi_M T$ upon cooling confirm a weak antiferromagnetic interaction between Co(II) centers and/or the spin−orbit coupling of the single Co(II) ion. The room-temperature effective magnetic moment per Co (4.70 μ_B) is much higher than the expected spin-only value for $S = 3/2$ (3.87 μ_B), attributed to the orbital contribution of the octahedral Co(II) ion. The temperature dependent *ac* susceptibility data show a maximum of the in-phase signal (χ') at 2.2 K and the absence of the out-of phase signal (χ''), indicating that compound **2** has an antiferromagnetic (AF) ground state (Figure S3, Supporting Information). The field-dependent magnetization at 1.8 K was also measured (Figure 14). The magnetization increases linearly below 12.53 kOe, then nonlinearly above 12.53 kOe, and reaches 3.67 Nβ at the highest measuring field of 70.20 kOe. The d(M/Nβ)/dH versus H curve indicates the occurrence of a two-step field-induced magnetic phase transition (Figure 14, inset). The first one occurs between 0 and 45.13 kOe with a critical field of 12.53 kOe. The M value at 45.13 kOe is 2.68 Nβ, which is close to that expected for one uncompensated Co(II) ion ($S_{eff} = 1/2$ and $g = 4.1-5.0$).[23] Hence, this step could be assigned to a transition from the antiferromagnetic ground state to a ferrimagnetic state. Above 45.13 kOe, compound **2** experiences a second-step transition from the ferrimagnetic state to a spin polarized state. The magnetization at 70.20 kOe (3.67

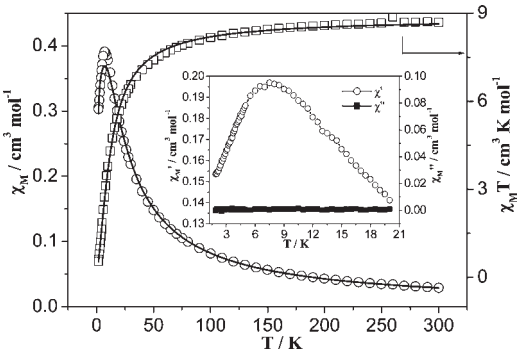

Figure 15. The χ_M and $\chi_M T$ vs T plots and zero-field ac magnetic susceptibility (inset) for **3**.

Nβ), however, is far from the saturation value anticipated for three Co(II) ions, suggesting that full polarization is not reached up to 70.20 kOe.

Compounds **1** and **2** show quite different magnetic properties, and both are also different from α-$Co_3(ImhedpH)_2(H_2O)_4 \cdot 2H_2O$[9b] with weak ferromagnetism at 2.6 K. The different magnetic behaviors should arise from their different structures, such as the structure of the inorganic layer and interlayer distance etc.

Figure 15 shows the χ_M and $\chi_M T$ vs T plots for compound **3**. The room temperature effective magnetic moment is 8.34 μ_B for Mn_2, close to the expected spin-only value for spin $S = 5/2$ with $g = 2.0$ (8.37 μ_B). In the temperature range of 30−300 K, the magnetic behavior follows the Curie−Weiss law with a Curie constant of 9.06 cm^3 K mol^{-1} and a Weiss constant of −11.09 K. The negative Weiss constant indicates a weak antiferromagnetic interaction between Mn(II) centers, which is further confirmed by the continuous decreasing of $\chi_M T$ upon cooling. The χ_M vs T curve shows a rounded peak at 7.0 K, typical for a low-dimensional antiferromagnetic compound. The temperature-dependent *ac* susceptibilities were further measured (Figure 15, inset). The in-phase signal (χ') shows a maximum at 7.5 K, while the out-of phase signal (χ'') does not exhibit any peak, suggesting that compound **3** has an antiferromagnetic ground state.

In the ladder-like structure of compound **3**, the Mn···Mn distance (3.351 Å) over μ_3-O5 is much shorter than those over the O−P−O bridges along the leg (5.482 Å) and the diagonal (4.574 Å). Thus, the magnetic susceptibility data can be analyzed by an isotropic dimer model for two $S = 5/2$ ions based on a Heisenberg Hamiltonian $H = -2JS_1S_2$:[17]

$$\chi_M = (2Ng^2\beta^2/kT)[\exp(2J/kT) + 5\exp(6J/kT) + 14\exp(12J/kT) + 30\exp(20J/kT) + 55\exp(30J/kT)]/[1 + 3\exp(2J/kT) \times 5\exp(6J/kT) + 7\exp(12J/kT) + 9\exp(20J/kT) + 11\exp(30J/kT)]$$

where $2J$ is the coupling constant and N, g, β, and k have their usual meanings. The best fit, shown as the solid lines in Figure 15, results in parameters $g = 2.01$ and $2J = -0.88$ cm^{-1}. The $2J$ value is comparable to those in compounds $[NH_3(CH_2)_nNH_3][Mn_2(hedpH)_2] \cdot 2H_2O$ [$2J = -0.67$ cm^{-1} ($n = 4$), −0.69 cm^{-1} ($n = 5$), −0.77 cm^{-1} ($n = 6$)] with ladder structures similar to that of **3**.[20] Since the Mn···Mn distance along the leg is much larger than that along the diagonal, **3** could be viewed as an antiferromagnetically coupled alternative chain from the

dx.doi.org/10.1021/ic1019668 |*Inorg. Chem.* 2011, 50, 2278–2287

magnetic point of view. The measurement of field-dependent magnetization at 1.8 K reveals that the $M/N\beta$ increases with a constant slope (line *a*) upon increasing the magnetic field below about 10 kOe, while it jumps up and then increases with the other slope (line *b*) above that field (Figure S4, Supporting Information). The magnetization at 70.20 kOe is 2.80 Nβ, far from the saturation value anticipated for a Mn(II) (5.00 Nβ).

Conclusion. We describe the syntheses and structures of three new compounds based on 2-(1-imidazole)-1-hydroxy-1,1′-ethylidenediphosphonic acid ($ImhedpH_4$), namely, β-$Co_3(ImhedpH)_2(H_2O)_4\cdot 2H_2O$ (**1**), $Co_3(ImhedpH)_2(H_2O)_4$ (**2**), and $Mn(ImhedpH_2)\cdot H_2O$ (**3**). It is found that the reaction temperature, pH value, and metal source play important roles in the formation of compounds **1**−**3**. Compound **1** has a three-dimensional open framework, in which imidazole groups are involved in coordination, while **2** and **3** show layer and chain structures, respectively, where imidazole groups are not coordinated to the metal ions. The structures of inorganic layers in **1** and **2** are different from that in α-$Co_3(ImhedpH)_2(H_2O)_4\cdot 2H_2O$.[9b] Same topologies have not been observed in other metal phosphonates. Magnetic studies reveal that compound **1** exhibits the coexistence of ferrimagnetism and field-induced transition from ferrimagnetism to a fully polarized state with a critical field of *ca.* 32.6 kOe. Compound **2** has an antiferromagnetic ground state, and experiences a two-step field-induced magnetic phase transition AF ground state to a ferrimagnetic state and then to a spin polarized state. For compound **3**, a low dimensional AF behavior is observed. Further work is in progress to synthesize new metal phosphonates with interesting physical properties.

■ ASSOCIATED CONTENT

Supporting Information. X-ray crystallographic files in CIF format for the four compounds, TG curves for compounds **1**−**3**, and field-dependent magnetization for compound **1**. This material is available free of charge via the Internet at http://pubs.acs.org.

■ AUTHOR INFORMATION

Corresponding Author

*E-mail: dkcao@nju.edu.cn (D.-K.C.), lmzheng@nju.edu.cn (L.-M.Z.). Fax: +86-25-83314502.

■ ACKNOWLEDGMENT

We thank the NSF of China (No. 90922006), NSF of Jiangsu Province (No. BK2009009), the National Basic Research Program of China (2007CB925102, 2010CB923402), and the NSF for the creative research group (No. 21021062) for financial support. We also thank Mr. Yong-Jiang Liu for crystal data collection and Prof. Dr. You Song for magnetic measurements.

■ REFERENCES

(1) (a) Clearfield, A. *Prog. Inorg. Chem.* **1998**, *47*, 371. (b) Miller, S. R.; Pearce, G. M.; Wright, P. A.; Bonino, F.; Chavan, S.; Bordiga, S.; Margiolaki, I.; Guillou, N.; Férey, G.; Bourrelly, S.; Llewellyn, P. L. *J. Am. Chem. Soc.* **2008**, *130*, 15967. (c) Brunet, E.; Alhendawi, H. M. H.; Cerro, C.; Mata, M. J.; Juanes, O.; Rodríguez-Ubis, J. C. *Angew. Chem., Int. Ed.* **2006**, *45*, 6918.

(2) (a) Ma, L.-Q.; Abney, C.; Lin, W.-B. *Chem. Soc. Rev.* **2009**, *38*, 1248. (b) Chessa, S.; Clayden, N. J.; Bochmann, M.; Wright, J. A. *Chem. Commun.* **2009**, 797. (c) Youngblood, W. J.; Lee, S. H. A.; Kobayashi, Y.; Hernandez-Pagan, E. A.; Hoertz, P. G.; Moore, T. A.; Moore, A. L.; Gust, D.; Mallouk, T. E. *J. Am. Chem. Soc.* **2009**, *131*, 926. (d) Bao, S.-S.; Ma, L.-F.; Wang, Y.; Fang, L.; Zhu, C.-J.; Li, Y.-Z.; Zheng, L.-M. *Chem.—Eur. J.* **2007**, *13*, 2333.

(3) (a) Mao, J.-G. *Coord. Chem. Rev.* **2007**, *251*, 1493 and references therein. (b) Liu, X.-G.; Zhou, K.; Dong, J.; Zhu, C.-J.; Bao, S.-S.; Zheng, L.-M. *Inorg. Chem.* **2009**, *48*, 1901. (c) Brunet, E.; Alhendawi, H. M. H.; Juanes, O.; Jiménez, L.; Rodríguez-Ubis, J. C. *J. Mater. Chem.* **2009**, *19*, 2494.

(4) (a) Monot, J.; Petit, M.; Lane, S. M.; Guisle, I.; Léger, J.; Tellier, C.; Talham, D. R.; Bujoli, B. *J. Am. Chem. Soc.* **2008**, *130*, 6243. (b) Amalric, J.; Mutin, P. H.; Guerrero, G.; Ponche, A.; Sotto, A.; Lavigne, J. P. *J. Mater. Chem.* **2009**, *19*, 141. (c) Adden, N.; Gamble, L. J.; Castner, D. G.; Hoffmann, A.; Gross, G.; Menzel, H. *Langmuir* **2006**, *22*, 8197.

(5) (a) Maheswaran, S.; Chastanet, G.; Teat, S. J.; Mallah, T.; Sessoli, R.; Wernsdorfer, W.; Winpenny, R. E. P. *Angew. Chem., Int. Ed.* **2005**, *44*, 5044. (b) Shanmugam, M.; Chastanet, G.; Mallah, T.; Sessoli, R.; Teat, S. J.; Timco, G. A.; Winpenny, R. E. P. *Chem.—Eur. J.* **2006**, *12*, 8777. (c) Langley, S.; Helliwell, M.; Sessoli, R.; Teat, S. J.; Winpenny, R. E. P. *Inorg. Chem.* **2008**, *47*, 497. (d) Baskar, V.; Gopal, K.; Helliwell, M.; Tuna, F.; Wernsdorfer, W.; Winpenny, R. E. P. *Dalton Trans.* **2010**, *39*, 4747.

(6) (a) Ma, Y.-S.; Li, Y.-Z.; Song, Y.; Zheng, L.-M. *Inorg. Chem.* **2008**, *47*, 4536. (b) Ma, Y.-S.; Song, Y.; Li, Y.-Z.; Zheng, L.-M. *Inorg. Chem.* **2007**, *46*, 5459.

(7) (a) Sun, Z.-M.; Prosvirin, A. V.; Zhao, H.-H.; Mao, J.-G.; Dunbar, K. R. *J. Appl. Phys.* **2005**, *97*, 10B305. (b) Brockman, J. T.; Stamatatos, T. C.; Wernsdorfer, W.; Abboud, K. A.; Christou, G. *Inorg. Chem.* **2007**, *46*, 9160.

(8) (a) Gutschke, S. O. H.; Price, D. J.; Powell, A. K.; Wood, P. T. *Angew. Chem., Int. Ed. Engl.* **1999**, *38*, 1088. (b) Bellitto, C.; Federici, F.; Colapietro, M.; Portalone, G.; Caschera, D. *Inorg. Chem.* **2002**, *41*, 709. (c) Kong, D.; Li, Y.; Ouyang, X.; Prosvirin, A. V.; Zhao, H.; Ross, J. H.; Dunbar, K. R.; Clearfield, A. *Chem. Mater.* **2004**, *16*, 3020. (d) Yang, B.-P.; Prosvirin, A. V.; Guo, Y.-Q.; Mao, J.-G. *Inorg. Chem.* **2008**, *47*, 1453.

(9) (a) Ma, Y.-S.; Song, Y.; Du, W.-X.; Li, Y.-Z.; Zheng, L.-M. *Dalton Trans.* **2006**, 3228. (b) Cao, D.-K.; Li, Y.-Z.; Zheng, L.-M. *Inorg. Chem.* **2007**, *46*, 7571. (c) Guo, L.-R.; Zhu, F.; Chen, Y.; Li, Y.-Z.; Zheng, L.-M. *Dalton Trans.* **2009**, 8548.

(10) (a) Cao, D.-K.; Xie, X.-J.; Li, Y.-Z.; Zheng, L.-M. *Dalton. Trans.* **2008**, *46*, 5008. (b) Zhang, Z.-C.; Zheng, L.-M. *Inorg. Chem. Commun.* **2008**, *11*, 1243.

(11) (a) Yin, P.; Gao, S.; Zheng, L.-M.; Wang, Z.; Xin, X.-Q. *Chem. Commun.* **2003**, 1076. (b) Zheng, L.-M.; Gao, S.; Song, H.-H.; Decurtins, S.; Jacobson, A. J.; Xin, X.-Q. *Chem. Mater.* **2002**, *14*, 3143. (c) Wang, P.-F.; Bao, S.-S.; Zhang, S.-M.; Cao, D.-K.; Liu, X.-G.; Zheng, L.-M. *Eur. J. Inorg. Chem.* **2010**, 895.

(12) (a) Yin, P.; Zheng, L.-M.; Gao, S.; Xin, X.-Q. *Chem. Commun.* **2001**, 2346. (b) Ying, S.-M.; Mao, J.-G. *Cryst. Growth Des.* **2006**, *6*, 964.

(13) (a) Zheng, L.-M.; Song, H.-H.; Xin, X.-Q. *Comments Inorg. Chem.* **2000**, *22*, 129. (b) Liu, F.-Y.; Roces, L.; Ferreira, R. A. S.; Granda, S. G.; Garcia, J. R.; Carlos, L. D.; Rocha, J. *J. Mater. Chem.* **2007**, *17*, 3696. (c) Chen, Z.; Zhou, Y.; Weng, L.; Zhao, D. *Cryst. Growth Des.* **2008**, *8*, 4045.

(14) Mao, J.; Mukherjee, S.; Zhang, Y.; Cao, R.; Sanders, J. M.; Song, Y.; Zhang, Y.; Meints, G. A.; Gao, Y. G.; Mukkamala, D.; Hudock, M. P.; Oldfield, E. *J. Am. Chem. Soc.* **2006**, *128*, 14485 and references therein.

(15) (a) Freire, E.; Vega, D. R.; Baggio, R. *Acta Crystallogr., Sect. C* **2010**, *C66* (6), m166. Freire, E.; Vega, D. R.; Baggio, R. *Acta Crystallogr., Sect. C* **2010**, *C66* (4), m122. Freire, E.; Vega, D. R.; Baggio, R. *Acta Crystallogr., Sect. C* **2010**, *C66* (1), m13. (b) Freire, E.; Vega, D. R. *Acta Crystallogr., Sect. E* **2009**, *E65* (11), m1430. Freire, E.; Vega, D. R. *Acta Crystallogr., Sect. E* **2009**, *E65* (11), m1428.

(16) (a) Jiang, Y.; Zhang, X. Q.; Xu, Z. R. *Chin. J. Pharm.* **2004**, *35* (4), 204. (b) Jiang, Y.; Zhang, X. Q.; Xu, Z. R. *Huaxi J. Pharm.* **2005**, *20* (1), 29.

(17) Kahn, O. *Molecular Magnetism*; VCH: New York, 1993.

(18) *SAINT*; Siemens Analytical X-ray Instruments: Madison, WI, 1996.

(19) *SHELXTL Reference Manual*, version 5.0; Siemens Industrial Automation, Analytical Instruments: Madison, WI, 1997.

(20) Song, H.-H.; Yin, P.; Zheng, L.-M.; Korp, J. D.; Jacobson, A. J.; Xin, X.-Q. *J. Chem. Soc., Dalton Trans.* **2002**, 2752.

(21) Gong, Y.; Tang, W.; Hou, W.; Zha, Z.; Hu, C. *Inorg. Chem.* **2006**, *45*, 4987.

(22) Zhang, Z.-C.; Bao, S.-S.; Zheng, L.-M. *Inorg. Chem. Commun.* **2007**, *10*, 1063.

(23) (a) Drillon, M.; Coronado, E.; Belaiche, M.; Carlin, R. L. *J. Appl. Phys.* **1988**, *63*, 3551. (b) Robinson, W. K.; Friedberg, S. A. *Phys. Rev.* **1960**, *117*, 402.